

# COMPUTATIONAL ANALYSIS FOR FLAPPING WING BY COUPLED CFD AND CSD SOLUTIONS

Namhun Lee\*, Seungsoo Lee\*, Haeseong Cho\*\*, Jun-Young Kwak\*\*\*, and SangJoon Shin\*\*  
\*Inha University, \*\*Seoul National University, \*\*\*Korea Aerospace Research Institute

**Keywords:** *Flapping wing analysis, CFD-CSD coupling*

## Abstract

*For a flapping wing micro air vehicle (FWMAV), flexibility of the wing structure induces a crucial effect on the vehicle performance. This paper presents an accurate computational approach to simulate flapping wings by coupling between CFD and CSD. For the fluid structure interaction (FSI), a finite volume based preconditioned Navier-Stokes solver with a non-linear structural model based on the geometrically exact beam formulation is used. Aeroelastic analysis is performed, and the results are compared with the experimental results. For the realistic flapping wing analysis, by considering their detailed configuration, the finite element analysis, beam and shell, based on a co-rotational (CR) theory is developed in parallel.*

## 1 Introduction

As the operating Reynolds number of the micro air vehicle (MAV) decreases gradually, many complex flow phenomena can take place within the boundary layer, which can affect the performance of the lifting surface. Therefore, researchers are facing entirely new challenges to solve these problems in this flight regime [1].

Early studies have focused on both the mechanism of the flapping motions and the aerodynamics of the flapping wings due to prescribed flapping motions. Taira and Colonius [2] presented results of numerical simulations for three-dimensional separated flows around low-aspect ratio wings at low Reynolds numbers. They focused the unsteady nature of the separated flows, and vortex dynamics which affect the aerodynamic forces. However, their

study was performed only for rigid wings. Recent studies focused more on fluid structure interaction (FSI) analysis as the effects of wing flexibility on the aerodynamic performance are highlighted.

Smith [3] and Hanamoto et al. [4] studied the effects of the wing flexibility on the aerodynamics of insects' wings by using the FSI analysis. Both investigations were performed with a low order aerodynamics and structural model. Singh [5] discussed a computational aeroelastic framework for bio-inspired flapping wings. A finite element structural analysis of the wings was used with an unsteady aerodynamic analysis. He measured the propulsive forces of various wings with a flapping-pitching mechanism within a few combinations of the stroke parameters.

Recently, Chimakurthi et al. and Gordnier et al. [6, 7, 8] built a numerical framework to facilitate the aeroelastic simulations of flexible flapping wings at variable fidelity levels. Those works focused on the interactions between the fluids and the flexible flapping wings. A finite volume based Navier-Stokes fluid dynamics solver and a finite-element structural dynamic solver based on geometrically nonlinear composite beam were included in their framework. They obtained good agreements between the numerical results and the results of the experiment by Heathcote et al. [9]. Comparisons were made in terms of the instantaneous vertical tip displacement and the thrust force on the flexible wings.

This paper suggests an analytical framework for aeroelastic simulation of flapping wings. It is capable of predicting more accurate and reliable results in both structural and aerodynamic aspects, such as internal structural

loads and aerodynamic quantities. A finite volume based preconditioned Navier-Stokes solver and a non-linear structural model based on the geometrically exact beam formulation are used. In addition, the radial basis function (RBF) interpolation method is adopted to generate computational grids around flapping wings. Also, a non-linear beam based on a corotational (CR) framework is developed in parallel, which will improve drastically the accuracy of the present structural analysis. The CR structural analysis will be completed and implemented within the present aeroelastic analytical framework.

## 2 Formulations and Implementation

### 2.1 Aerodynamic model

#### 2.1.1 Governing equations

To analyze flows around the flapping wings at low Mach and Reynolds number regime, the three-dimensional preconditioned Navier-Stokes equations are chosen as governing equations. A differential form of the non-dimensional governing equations with an artificial time derivative term can be written as

$$\Gamma \frac{\partial Q_p}{\partial \tau} + \frac{\partial W}{\partial t} + \nabla \cdot \vec{F} = \nabla \cdot \vec{F}_v, \quad (1)$$

where  $W$  is the conservative solution vector,  $Q_p$  is the primitive solution vector,  $\vec{F}$  is the inviscid flux vector, and  $\vec{F}_v$  is the viscous flux vector. Notice that the fictitious time derivative term is added for accurate unsteady computations. A preconditioning matrix,  $\Gamma$  of Weiss and Smith [10] is adopted for accurate and efficient computations for low Mach number flows.

#### 2.1.2. Numerical schemes

The numerical algorithm used in this paper is based on the finite volume method (FVM). For the discretization of the inviscid flux vector, Roe's approximated Riemann solver [11] in conjunction with MUSCL extrapolation is used. Van Albada's limiter is also adopted to obtain

the higher spatial accuracy while maintaining the total variation diminishing (TVD) property. The derivatives of the solution vectors are computed at the cell interfaces by applying the gradient theorem over an auxiliary cell. These derivatives are used to compute the viscous flux vector, which is equivalent to the second order central difference method on a regular grid.

For the unsteady flow analyses, a dual time stepping method in conjunction with approximate factorization-alternate direction implicit (AF-ADI) method is used to discretize the fictitious time derivative term of the governing equations.

#### 2.1.2 Deformation of grid

A deforming grid technique is required to automatically generate a grid system inside the flow field in order to predict the flow induced by the flapping motion of the wing. A rigid grid shearing method and a radial basis function (RBF) interpolation are also applied.

##### Rigid grid shearing

The rigid grid shearing method can be used for simple topology grid systems, such as a C-H type. First, the new positions of the wing surface grid points are computed by a rigid translation and rotation at a span location. The grid points inside of the flow field and along the far-field boundaries are obtained by shearing the grid with the same amount of the translation and rotation of the wing surface.

This method is simple and fast compared to the other techniques. However, it can maintain the grid quality up to a moderate deformation. Furthermore, it ignores sectional rotation due to the bending deformation.

##### RBF interpolation method

A good quality grid can be created from the deformed wing surface grid with the RBF interpolation method [12, 13]. Figure 1 shows the result of the grid deformation applied to C-H type wing grid system which has a translational as well as a rotational deformation. Note that the outer boundaries of the grid system are kept unchanged. The surface grid points of the wing, however, deform, so that the interior grid points

at constant  $k$  plane also deform to maintain good quality of grid.

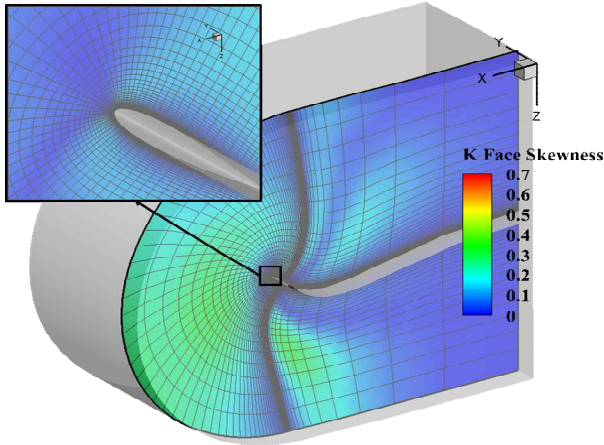


Fig. 1. Grid deformation result, C-H type wing grid system; RBF interpolation

For the efficient construction of the interpolation function, a greedy algorithm suggested in [14] is used. The conjugate gradient method is used to solve the linear equation.

### 2.1.3 Geometric conservation law

For an evaluation of the volume of computational cells in deformation, only geometric consideration is not enough to ensure that the uniform flow is a solution to the Navier-Stokes equations [15]. The geometric conservation law (GCL) is adopted to alleviate the problem.

## 2.2 Structural model

### 2.2.1 Geometrically exact beam (GEB) analysis

The three-dimensional, geometrically nonlinear elastic problem of the beam element is divided into a two-dimensional cross sectional analysis and a one-dimensional beam analysis. The present nonlinear intrinsic beam formulation was originally suggested by Hodges [16]. Shang implemented this formulation in the frequency domain [17] and Cheng further modified it for implementation in time domain [18].

The resulting nonlinear beam formulation is based on a small amount of strain and large deformation with finite rotation. The variational

formulation is derived from Hamilton's principle.

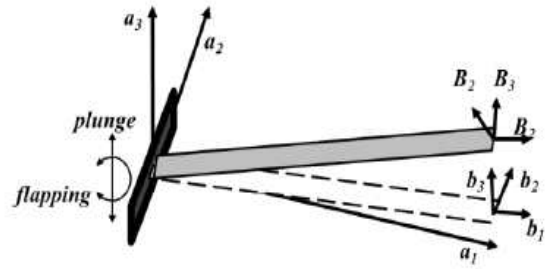


Fig. 2. Coordinate system of the present beam analysis

Figure 2 shows coordinates used in this formulation. In Fig. 2, the frame 'B' is the deformed beam reference frame and 'b' is the undeformed beam reference frame. A mixed variational formulation is devised using the Lagrange multipliers. Thus this formulation maintains the generalized displacements, strains, forces, and momenta as independent variables. By using the present structural model, it becomes possible to obtain accurate predictions of the internal forces and moments without usage of the higher order shape functions. The final form of the governing equation is as follows:

$$F_S(X, \dot{X}) - F_L = 0, \quad (2)$$

where  $F_S$  is the structural operator,  $F_L$  is the aerodynamic operator, and  $X$  is the unknown structural state variables. To solve the present nonlinear equation, the Newton-Raphson method is employed. The second-order backward Euler method with the previous two time steps is used for time integration.

### 2.2.2 CR finite elements analysis

Generally, the flapping wing's configuration is not slender and the wing consists of the vein and wing membrane. Regarding the vein, its section geometry is complex. The warping, which is possible to generate due to the complex section geometry of the vein, is needed to be considered as well. In order to consider those features, and to overcome the limitation of the one-dimensional beam approach, a precise structural analysis is required. In the present research, a nonlinear finite element, i.e. beam and shell, based on the

co-rotational (CR) framework [19] will be adopted. Regarding the more accurate beam analysis including the warping DOF, there exists a formulation based on the geometrically exact beam model [20]. However, it is more complicated than the formulation based on the CR framework is. Currently, a unified analytical CR framework is developed and applied to the beam analysis with the warping degree of freedom (DOF) and shell analysis.

The CR framework is independent of the specific local element formulation. Thus, a large number of the existing robust and accurate geometrically linear elements can be reused and extended to geometrically non-linear analysis.

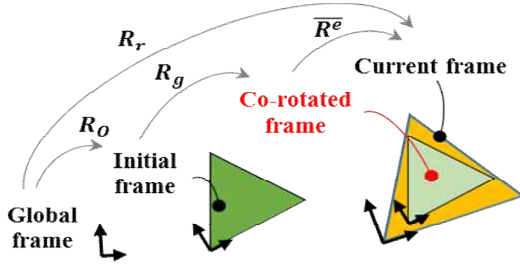


Fig. 3. Coordinate system of the present beam analysis

Figure 3 shows the coordinate system of the framework. The CR framework decouples the geometrical non-linearity from the material response of the element. Due to the assumption that the pure deformation is small in the local CR frame, the geometrically linear finite element formulation can be used to obtain the element stiffness matrix and internal force vector in the local CR frame. A consistent transformation of element stiffness matrix and internal force vector from the local CR frame to the global coordinate system is used, while the geometrically nonlinear effects are considered. Details of its mathematics, presented in Ref. [19], can be summarized as follows:

$$d_g = E^T d_l, \quad (3)$$

$$\begin{aligned} f_g &= E^T f_l, \\ K_g &= E^T K_l E + \partial(E^T f_l) / \partial d_g, \end{aligned} \quad (4)$$

where  $d$ ,  $f$  and  $K$  are the displacement, the internal force vectors and the stiffness matrix,

respectively. Also,  $E$  and  $\partial(E^T) / \partial d_g$  represent transformation matrices. Those matrices are constructed with regard to the element frame in order to re-express displacement, internal force vectors and stiffness matrix.

By following the above manner as well as the consideration of nodal DOF, it is possible to compose various nonlinear finite elements. This suggests that the procedure in Eqs. (3) and (4) will be applicable to the CR beam and shell element by only expanding the transformation matrices from 14 (for beam element with a warping DOF) to 18 DOF (for 3-nodes shell element). Also, the existing high performance geometrical linear elements can be used [21, 22].

### 2.3 CFD-CSD coupling procedure

To couple the aerodynamic model with the structural model, an implicit coupling method is adopted. In the implicit coupling method, aerodynamics/structure coupled solutions are determined iteratively by exchanging data once every CFD-CSD sub-iteration.

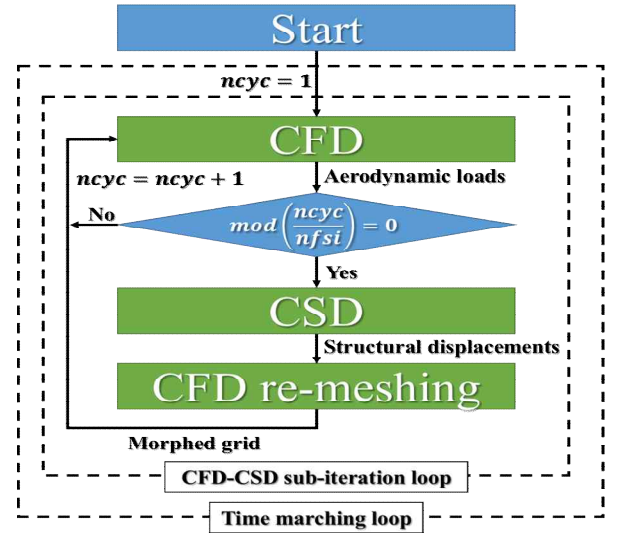


Fig. 4. A diagram of the implicit coupling approach

In this paper, a parameter,  $nfsi$ , is used to control the frequency of the data exchange in the sub-iteration loop to save the computational time. A diagram of the implicit coupling method is presented in Fig. 4.

A linear interpolation is applied across the fluid-structure interface. The distributed loads in

CFD analysis will be interpolated by the linear interpolation and transferred to the nodal forces in CSD analysis.

### 3 Numerical results

In this section, the present aeroelastic analysis method is to be validated. In order to achieve the goal, verifications of each aerodynamic and structural models are conducted separately. The results of the aerodynamic validation (rigid wing case) are compared with the aeroelastic results. The present results are compared with experimental results by Heathcote et al. [9] and numerical results by Gordnier et al. [8].

**Table. 1. Experimental conditions**

Classification	Value	Classification	Value
Reynolds number	30000	Plunge amplitude	0.0175m
Flow velocity	0.3m/s	Prescribed motion	Cosine
Water density	1000 kg/m <sup>3</sup>	Reduced frequency	0~1.82

**Table. 2. Properties of the wings**

Classification	Rigid	Flexible	Highly Flexible
Semi-span width	0.3m	0.3m	0.3m
Chord length	0.1m	0.1m	0.1m
Thickness	-	0.001m	0.001m
Poisson's ratio	-	0.3	0.3
Material density	-	7800 kg/m <sup>3</sup>	2700 kg/m <sup>3</sup>
Young's modulus	-	210 GPa	40 GPa

Heathcote et al. conducted an experimental study for the rectangular cantilever wings (NACA-0012 cross-section) with three different levels of flexibility property. The experimental conditions and the geometric configuration are shown in Tables 1 and 2, respectively.

#### 3.1 Structural results

Two structural analytical models are developed: the geometrically exact beam and CR nonlinear finite elements. Currently, the

present GEB beam analysis is capable of the time transient analysis and CR shell operates only in static condition. Validation of each structural analysis is conducted.

##### 3.1.1 Plate in a time-varying plunge motion

To verify the present structural analysis, a plate in time-varying plunge motion is analyzed. Plunging frequency of 1.78Hz is chosen. The description of this analysis is presented in Table. 3 and Fig. 5.

**Table. 3. Analysis condition of the plate**

Classification	Value	Classification	Value
Length	0.3m	Poisson's ratio	0.3
Width	0.1m	Material density	7800 kg/m <sup>3</sup>
Thickness	0.001m	Young's modulus	210 GPa
Plunge amplitude	0.0175m	Plunge motion	1-cosine

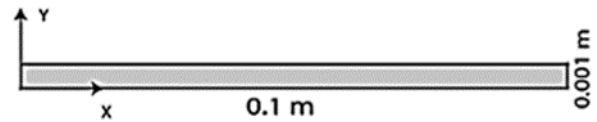


**Fig. 5. Configuration of the plate**

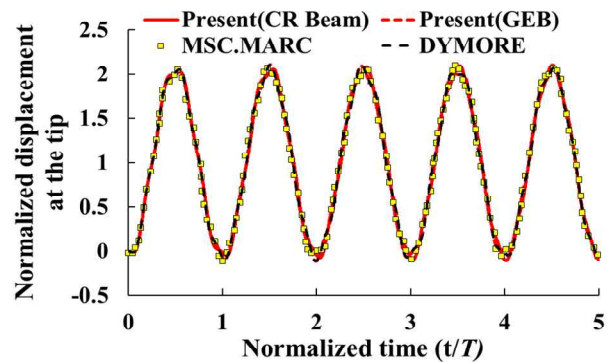


**Fig. 6. Comparison of the structural results with DYMORE and MSC.MARC**

Using such condition, both GEB and CR beam are validated. The results of their nonlinear response in z-direction are normalized by the plunging amplitude, and compared with the numerical results by DYMORE [23] and MSC.MARC (Fig. 6). The results from the present analysis show a good correlation with

those predicted by DYMORE and MSC.MARRC, within the difference as small as 0.38% and 0.25%, GEB and CR beam, respectively.

3.1.2 Cantilevered plate in a static tip load condition.

The CR non-linear shell analysis is further validated by comparing its results with those from NASTRAN for a static condition. A cantilevered plate, under the various transverse tip-loads, is analyzed (Fig. 7). Its tip-load is increased until the geometrically non-linear behavior becomes severe. Regarding the nonlinear behavior, shortening effect, length reduction of the beam, is shown clearly, as the tip-load increases (Fig. 8).

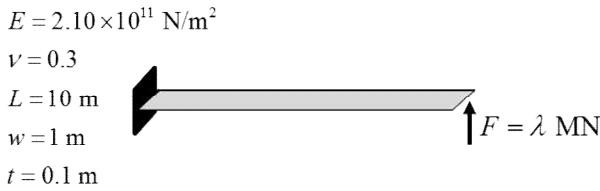


Fig. 7. Schematic of the cantilevered plate analysis

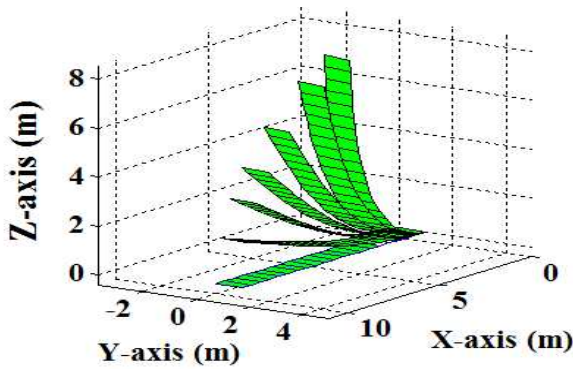


Fig. 8. Configuration of deformed plate

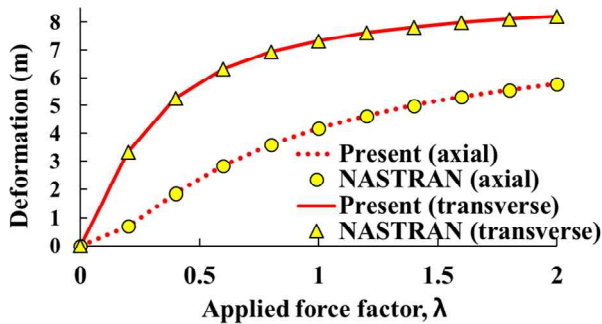


Fig. 9. Comparison of the structural predictions for a cantilevered plate

Figure 9 shows the comparison of the deflection predictions between the present and NASTRAN. It shows good agreements with those by NASTRAN, within difference as small as 0.2% (axial) and 0.4% (transverse).

3.2 Aeroelastic results

3.2.1 Flexible wing results for  $k_G=1.82$

The flexible wing under the prescribed plunging motion is analyzed to verify the present aeroelastic analysis. Time transient computations are performed for 340 time-steps multiplied by a period of the plunge motion. The number of sub-iterations is 30. Both grid deforming methods are used. However a sectional rotations due to bending are included in the case of the RBF only. Based on the convergence test,  $nfsi$  of 3 is chosen to ensure the accuracy of the solution as well as the efficiency.

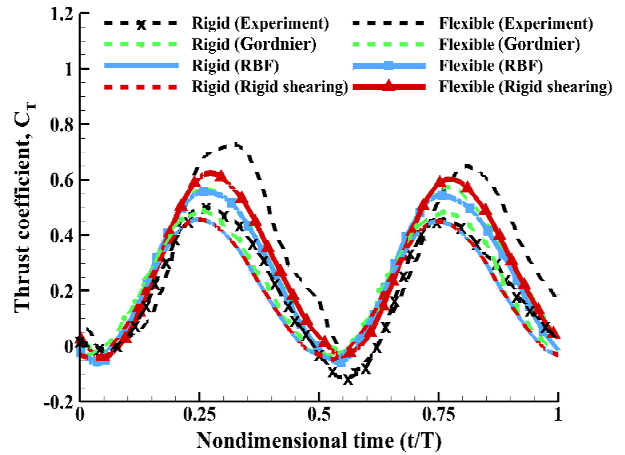


Fig. 10. Thrust response of the flexible wing

Figure 10 shows the thrust coefficient response. The increase in thrust due to the flexibility of the wing is well captured with the present analysis. However, the present analysis predicts the maximum thrust lower than that obtained in the experimental result. The numerical result by Gordnier [8] also underestimated the maximum thrust. Also, it is found that the maximum thrust decreases when the sectional rotations are taken into account.

Figure 11 compares the lift response, while Fig. 12 compares the tip displacement. As shown in Fig. 11, the maximum lift for the

flexible wing is 26% higher than that for the rigid wing. The wing tip response at reduced frequency of 1.82 is compared in Fig. 12. The present result shows a good correlation with that of the experiment, with difference as small as 0.2% in peak to peak.

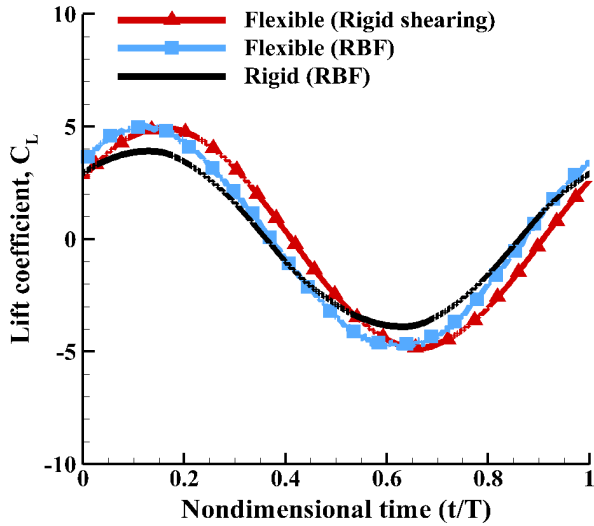


Fig. 11. Effect of structural flexibility on the lift generation

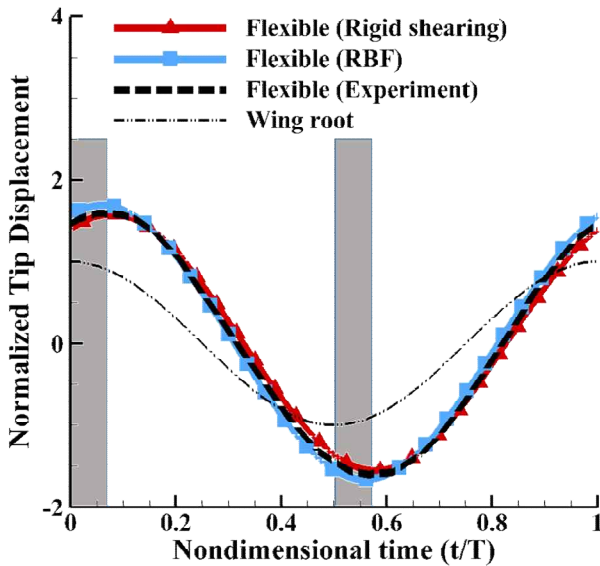


Fig. 12. Comparison of the tip displacement (Flexible)

Liu and Bose [24] found that in-phase motions yielded a significant increase in thrust and lift. Moreover out-of-phase motions yielded a decrease in thrust and lift. In Fig. 12, the gray highlighted regions suggest that the phase of the flexing motion relative to the plunge is out of phase. From the figure, it is found that the tip

displacement is in-phase during most of the stroke. This explains the increase in thrust as well as the increase in lift due to the flexibility of the wing.

Figures 11 and 12 also show the inclusion of the sectional rotations lead the phase shift of the responses of the lift and tip displacement. This tendency will require further investigation.

Furthermore, the wing internal load distribution, following the spanwise direction, is predicted. The present prediction shows the phase shift in the axial force distribution. Also, the chordwise force response shows increased frequencies (almost by twice) by following the thrust response. Only the present results are shown in Figs. 13 and 14, chordwise force and flapwise force, respectively.

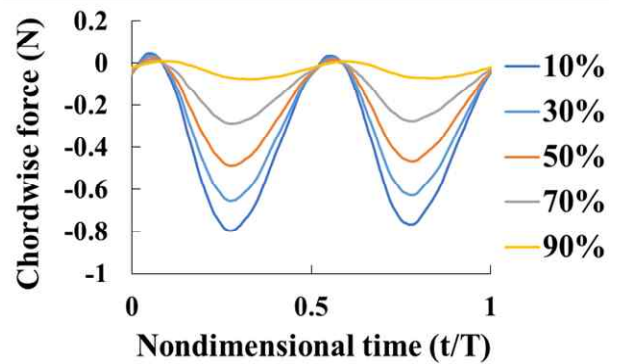


Fig. 13. Chordwise force distribution upon the wing

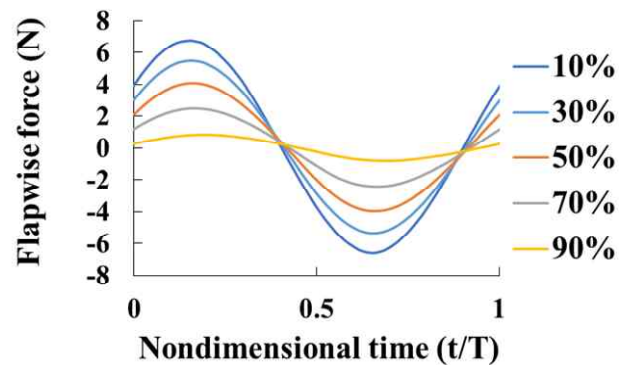


Fig. 14. Flapwise force distribution upon the wing

### 3.2.2 Highly flexible wing results for $k_G=1.82$

In this section, the highly flexible wing under the prescribed plunging motion is analyzed. In the experiment, thrust exhibits high frequency about  $St=10.21$ . However, this case is more challenging [6, 7, 8]. This paper, therefore,

focuses on the trend of the thrust change upon the spanwise flexibility. Approximately 340 time-steps is employed over each period of the plunging motion, based on the convergence test. For this computation, the number of sub-iterations is 30 and  $nfsi$  of 1 is chosen to ensure the accuracy of the solution. Sectional rotations due to bending are not included. Thus, both grid deforming methods are used and the results of each other are compared.

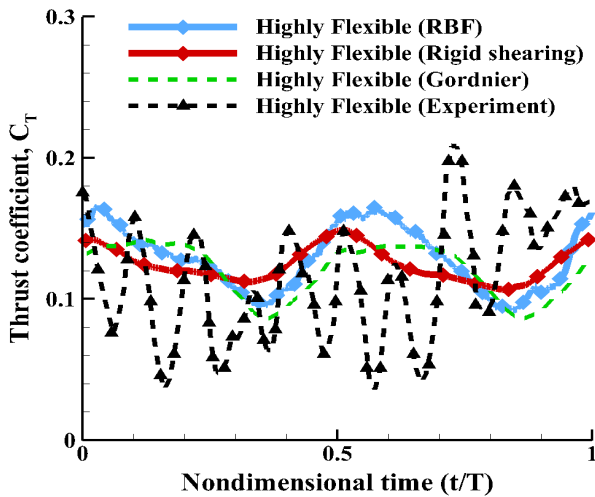


Fig. 15. Thrust response of the highly flexible wing

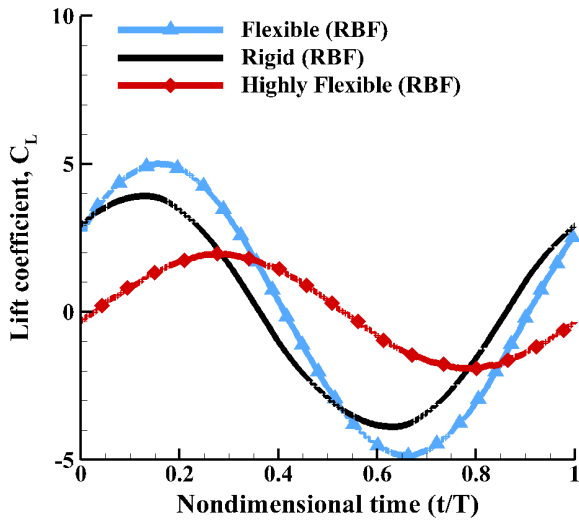


Fig. 16. Effect of structural flexibility on the lift generation

Figure 15 shows the thrust coefficient response. It does not exhibit high frequency response. However, the thrust reduction due to the flexibility of the wing is well captured. The averaged thrust is 0.129 (RBF) and 0.124 (rigid

shearing). And the differences relative to the experimental result are 17% and 13%, respectively. Figure 15 shows that there exist discrepancy between the RBF and rigid shearing result, unlike the previous flexible wing case. The thrust response with the RBF interpolation method is closer to that by Gordnier.

As shown in Fig. 16, the maximum lift for the highly flexible wing is lower than that for the rigid wing. In this paper, the maximum lift and the phase discrepancy are 50% lower and 36% smaller than those for the rigid wing, respectively. The results of the thrust and lift responses show that the maximum thrust occurs near the minimum lift.

Figure 17 shows the wing tip displacement response for the highly flexible wing. In the figure, the present result is compared with the experiment as well as that by Gordnier. The present result shows good correlations with that from the experiment, within the difference as small as 2.3% (RBF) and 11.6% (rigid shearing) in peak to peak. Also, there is a phase discrepancy of the response between the present prediction and the experimental result with the difference as 7.6% (RBF) and 4.1% (rigid shearing). In this case, it is found that the tip displacement is out-phase in most areas, so that the decrease in thrust due to the flexibility of the wing can be explained.

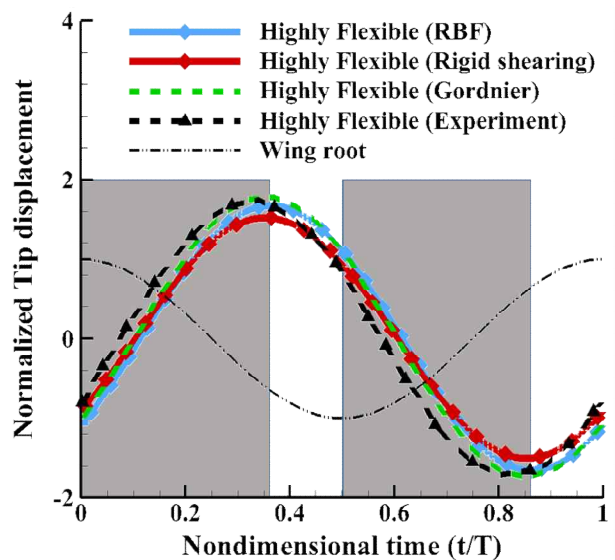


Fig. 17. Comparison of the tip displacement (Highly Flexible)

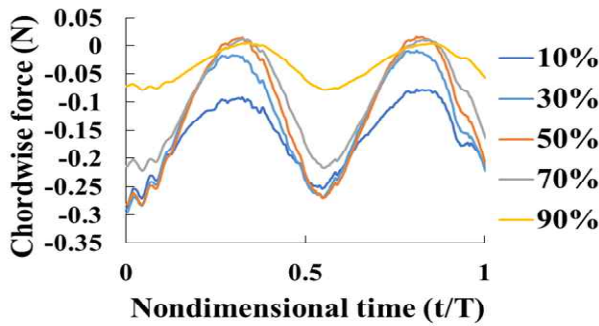


Fig. 18. Chordwise force distribution on the wing ( $k_G=1.82$ )

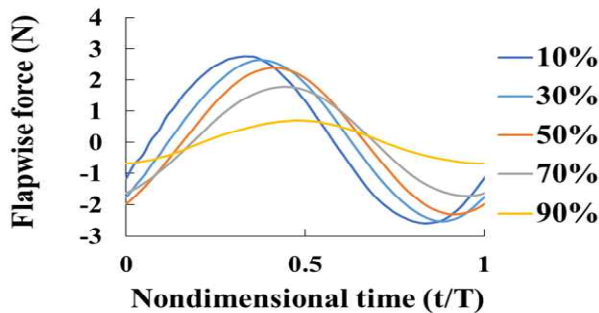


Fig. 19. Flapwise force distribution on the wing ( $k_G=1.82$ )

In addition to the tip displacement result, the wing internal load distribution along the spanwise direction is predicted as well. Only the present results are shown in Figs. 18 and 19, chordwise force and flapwise force, respectively. Regarding the present loads result upon the highly flexible wing, the phase shift along the spanwise direction is significantly observed by comparing with that from the flexible wing. Also, the chordwise force response shows increased frequencies (almost by twice) by following the thrust response. Comparing with the results upon the flexible wing, the magnitude of the loads is smaller than those for the flexible wing, because of the reduction in the aerodynamic forces. Due to the flexibility of the highly flexible wing, the elastic deflection is increased when it is compared with those of the flexible wing. Thus, the significant phase shift in the loads response along the wing spanwise direction is predicted.

#### 4. Concluding Remarks

In this paper, a CFD-CSD coupling framework is established. A preconditioned

Navier-Stokes solver is used for aerodynamic analysis, while a geometrically exact beam model is used for the structural analysis. Each solution is verified by using a rectangular NACA 0012 cross-section wing. The present aerodynamic and structural analyses are coupled by adopting an implicit coupling approach.

The aerodynamic and structural aspects of the coupled analysis are compared with the existing results. The present computational results are correlated well with the existing results. Especially, the tip response of the flexible wing shows a good correlation with that of the experiment. The difference is as small as 0.2% in peak to peak when compared with the experimental result. Also, the present analysis captures well the features observed in the experiments. The present analysis method provides internal loads of the wing directly, which gives more information for a design of the FWMAs.

In this paper a non-linear beam analysis based on the CR framework has been developed and validated. In the future, a more reliable analytical framework for the flapping wing will be constructed by applying the presently developed CR framework.

#### Acknowledgment

This work is supported by National Research Foundation of Korea (NRF) Grant funded by the Korean Government (2011-0029094).

#### References

- [1] Pines, D.J. and Bohorquez, F., "Challenges facing future micro-air-vehicle development," *Journal of aircraft*, Vol. 43, No.2, 2006, pp. 290-305.
- [2] Taira, K. and Colonius, T., "Three-dimensional flows around low-aspect ratio flat-plate wings at low Reynolds numbers," *J. Fluid Mech.*, Vol. 623, 2009, pp. 187-207.
- [3] Smith, M. J. C., "The Effects of Flexibility on the Aerodynamics of Moth Wings: Towards the Development of Flapping-Wing Technology," *33rd Aerospace Sciences Meeting and Exhibit*, Reno, Nevada, 1995.
- [4] Hamamoto, M., Ohta, Y., Hara, K., and Hisada, T., "Application of Fluid-Structure Interaction Analysis to Flapping Flight of Insects With Deformable

- Wings,” *Advanced Robotics*, Vol. 21, No. 1-2, 2007, pp. 1-21.
- [5] Singh, B., “Dynamics and Aeroelasticity of Hover Capable Flapping Wings: Experiments and Analysis”, Ph.D. Dissertation, Department of Aerospace Engineering, University of Maryland, College Park, Maryland, 2006.
- [6] Chimakurthi, S. K., Stanford, B. K., Cesnik, C. E. S. and Shyy, W., “Flapping Wing CFD/CSD Aeroelastic Formulation Based on a Corotational Shell Finite Element,” *AIAA-2009-2412, 50th AIAA / ASME / ASCE / AHS / ASC Structures, Structural Dynamics, and Materials Conference*, Palm Springs, CA, May 4-7, 2009.
- [7] Chimakurthi, S. K., Tang, J., Palacios, R., Cesnik, C. E. S. and Shyy, W., “Computational Aeroelasticity Framework for Analyzing Flapping Wing Micro Air Vehicles,” *AIAA Journal*, Vol. 47, No. 8, 2009, pp. 1865-1878.
- [8] Gordnier, R.E., Chimakurthi, S.K., Cesnik, C.E.S., Attar, P.J., “High-fidelity aeroelastic computations of a flapping wing with spanwise flexibility,” *Journal of Fluids and Structures*, Vol. 40, pp. 86-104, 2013.
- [9] Heathcote, S., Wang, Z. and Gursul, I., “Effect of Spanwise Flexibility on Flapping Wing Propulsion,” *Journal of Fluids and Structures*, Vol. 24, No. 2, 2008, pp. 183-199.
- [10] Weiss, J.M., and Smith, W.A., “Preconditioning applied to variable and constant density flows,” *AIAA Journal*, Vol. 33, No. 11, 1995, pp. 2050-2057.
- [11] Roe, P.L., “Approximate Riemann Solvers, Parameter Vectors, and Difference Schemes,” *Journal of Computational Physics*, Vol. 32, 1981, pp. 357-372.
- [12] Rendall, T.C.S., and Allen, C.B., “Unified fluid-structure interpolation and mesh motion using radial basis functions,” *Int. J. Numer. Meth. Engng.*, Vol. 74, Issue. 10, 2008, pp. 1519-1559.
- [13] Wright, G.B., “Radial basis function interpolation: numerical and analytical developments,” Ph.D. Dissertation, University of Colorado, Denver, USA, 2003.
- [14] Schaback, R., and Wendland, H., “Adaptive greedy techniques for approximate solution of large RBF systems,” *Numerical Algorithms*, Vol. 24, Issue. 3, 2000, pp. 239-254.
- [15] Thomas, P.D., and Lombard, C.K., “The Geometric Conservation Law A-Link Between Finite-Difference and Finite-Volume Methods of Flow Computation on Moving Grids,” *AIAA Paper 78-1208*, 1978.
- [16] Hodges, D. H., “A Mixed Variational Formulation Based on Exact Intrinsic Equations for Dynamics of Moving Beams,” *International Journal of Solids and Structures*, Vol. 26, No. 11, 1990, pp.1253–1273.
- [17] Shang, X., “Aeroelastic Stability of Composite Hingeless Rotors with Finite-State Unsteady Aerodynamics,” Ph. D. Dissertation, Georgia Institute of Technology, August 1995.
- [18] Cheng, T., “Structural Dynamics Modeling of Helicopter Blades for Computational Aeroelasticity,” M.S. Thesis, Massachusetts Institute of Technology, May 2002.
- [19] Felippa, C., “A Unified Formulation of Small Strain Corotational Finite Elements: I. Theory,” *Computational Methods in Applied Mechanics and Engineering.*, Vol. 194, pp. 2285-2335, 2005.
- [20] Yu, W., Hodges, D. H., Volovoi, V. V. and Fuchs, E. D., “A Generalized Vlasov Theory for Composite Beams,” *Thin-Walled Structures*, Vol. 43, pp. 1493-1511, 2005.
- [21] Battini, J. M., “Co-rotational Beam Elements in Instability Problems,” Ph. D. Dissertation, KTH Royal Institute of Technology, Stockholm, SWEDEN, 2002.
- [22] Khosravi, R., Ganesan, R. and Sedaghati, R., “An Efficient Facet Shell Element for Co-rotational Nonlinear Analysis of Thin and Moderately Thick Laminated Composite Structures,” *Computers and Structures*, Vol. 86, pp. 850-858, 2008.
- [23] Bauchau, O. A., *DYMORE Users’ Manual*, School of Aerospace Engineering, Georgia Inst. of Technology, Atlanta, GA, May 2006
- [24] Liu, P., and Bose, N., “Propulsive Performance from Oscillating Propulsors with Spanwise Flexibility,” *Proceedings of the Royal Society London. Series A: Mathematical, Physical and Engineering Sciences*, 453, pp.1763-1770, 1997.

## Contact Author Email Address

mailto : slee@inha.ac.kr

## Copyright Statement

The authors confirm that they, and/or their company or organization, hold copyright on all of the original material included in this paper. The authors also confirm that they have obtained permission, from the copyright holder of any third party material included in this paper, to publish it as part of their paper. The authors confirm that they give permission, or have obtained permission from the copyright holder of this paper, for the publication and distribution of this paper as part of the ICAS 2014 proceedings or as individual off-prints from the proceedings.